Examining Interactions Between Kappa Opioid Receptors and Dopaminergic Transmission in the Striatum of Socially Monogamous Prairie Voles

Zubin Sedghi

A Thesis Submitted in Partial Fulfillment of the

Requirements for the Degree of Bachelor of Arts

With Honors in Neuroscience from

The University of Michigan

2012

Advisor: Dr. Brandon Aragona

Abstract

Prairie voles are an excellent model for studying the neurobiology of social attachment, forming life-long pair bonds characterized by sharing territory, bi-parental care, and selective aggression of novel conspecifics. Pharmacological studies indicate that aversive social encounters, like selective aggression, are mediated by interactions between the dynorphin/κ-opioid receptor (KOR) systems and specific mesolimbic dopamine (DA) receptor systems within the nucleus accumbens (NAc) shell. In other species, this interaction has been examined, but not in prairie voles. Combining receptor autoradiography and *in vitro* fast-scan cyclic voltammetry, we investigated KOR modulation of DA transmission across three distinct striatal regions of sexually naïve voles—the NAc shell, the NAc core, and caudate putamen. Our results reveal that KOR modulation of DA transmission is greatest in the lateral CP and decreases in caudal regions within the NAc. These results are an important first step for future studies to assess the neurobiology of social attachment.

Keywords: dopamine, kappa opioid receptors, prairie vole, striatum

Examining Interactions Between Kappa-Opioid Receptors and Dopaminergic Transmission in the Striatum of Socially Monogamous Prairie Voles

With regards to mammalian mating behavior, monogamy is a rare trait; only in approximately 3-5% of all mammalian species does the male choose a monogamous mating strategy (Dewsbury, 1987). Although human social behavior is highly variable among individuals and cultures, the human species exhibits the ability to form enduring and selective social attachments (Atzil, 2011) and the presence of stable social bonds is critical for human mental health (Ravitz et al., 2010). Thus, finding and characterizing an effective animal model to examine this behavior is of particular interest for comparative studies, as it provides insight into underlying neurobiology of social attachment (Aragona & Wang, 2004). A common burrowing rodent, the prairie vole (*Microtus ochrogaster*) has been chosen as an excellent candidate for this line of research because of its penchant for monogamous pair bonding (Carter & Getz, 1993).

Behaviorally, two requirements must be met to ensure that a proper pair bond has been formed. Initially, a vole must develop preference for their mating partner. In the laboratory, this social choice is assessed via a partner preference test, which examines whether one member of the mating pair prefers their partner to a novel conspecific of the opposite sex (Williams et al., 1992). Once the pair reliably cohabitates, the second requirement is that the pair bond must be maintained by selective aggression towards other, unfamiliar voles (i.e. 'selective aggression'). This behavior is demonstrated experimentally through selective aggression testing, typically assayed using a resident-intruder test in which an unfamiliar vole is added to the cage of a mating pair and both aggressive and affiliative behaviors are assessed (Carter & Getz, 1993; Winslow et al.,

1993; Aragona et al., 2006). Taken together, partner preference and selective aggression provide approximate laboratory assessments of pair bonding (Aragona et al., 2006; Aragona & Wang, 2009).

Neurobiologically, mesolimbic dopamine (DA), an endogenous neurotransmitter that plays a key role in motivational behavior (Becker et al., 2001; Berridge & Robinson, 1998; Kelley & Berridge, 2002), is a critical neural substrate for proper functioning of prairie vole social attachment (Aragona et al., 2006). Both hallmarks of pair bonding—partner preference and selective aggression—rely on striatal dopaminergic activity. Specifically, within the nucleus accumbens (NAc) shell, activation of high affinity D_2-like DA receptors initiates the formation of partner preference, whereas low-affinity D_1-like activation prevents it (Aragona et al., 2006). Furthermore, once pair bonds have been established, neuroanatomical reorganization occurs in the NAc shell. D_1-like receptors become up-regulated in pair bonded males which, when blocked experimentally, attenuates selective aggression (Aragona et al., 2006). Thus, the recruitment of additional D_1-like receptors in pair bonded males act as a mechanistic one-two punch by not only preventing formation of new bonds with other conspecifics, but also promoting their aggressive rejection.

These opposing behavioral outcomes by activation of different DA receptor subtypes is intriguing because there is an analogous 'biochemical mirroring' in their intracellular, downstream signals. When DA binds to D_2-like receptors, cyclic adenosine monophosphate (cAMP) production decreases through the action of an inhibitory g-protein cascade. Conversely, D_1-like receptor activation increases cAMP production via activation of a stimulatory g-protein cascade (Aragona & Wang, 2007; Missale et al.,

1998). Downstream, cAMP promotes the production of dynorphin (DYN) (Gerfen et al., 1991), the endogenous ligand for κ-opioid receptors (KORs) (Chavkin et al., 1982), which is known to inhibit dopaminergic input in the striatum (Chefer et al, 2005).

Two of the main players of this biochemical loop, DYN and KORs, constitute the κ-opioid system. As mentioned above, activation of KORs reduces DA transmission and it has been suggested that this, at least in part, contributes to a reduction in motivational states, and perhaps even the dysphoric and aversive components of stressful states (Land et al., 2008). Congruently, a recent finding in our lab demonstrates that, in prairie voles, the KOR system mediates aversive social interactions, as determined by resident intruder assays of selective aggression, one of the important characteristics of an established pair bond. Specifically, blockade of KORs within the shell of the NAc inhibits selective aggression (Resendez et al., in press). Thus, in addition to the important role of DA alone, KORs are also critical for pair bond maintenance.

Still, many of the striatal details of the KOR/DA interaction remain unknown. While many studies have assessed KOR distribution in other species like humans, horses, guinea pigs, rabbits, rats, and mice (Mansour et al., 1987; Mansour et al., 1988; Quirion et al., 1987; Robson et al., 1985; Thomasy et al., 2007; Wang et al., 2011), the exact action and distribution of KORs in the prairie vole has yet to be carefully investigated. So, in order to assess the behavioral implications of social attachment on a neuroanatomical level, the first step must be to systematically analyze and understand the striatal organization of KORs and the effect of KOR activation on DA transmission in sexually naïve, control prairie voles.

In this study, we integrate techniques based in neurobiology and neurochemistry to characterize the topography of KOR distribution and the resulting effects on DA release in several sub-regions within the striatum. First, we visualized KOR binding through receptor autoradiography and then utilized *in vitro* fast-scan cyclic voltammetry (FSCV) to measure how DA release was altered in three brain regions—the caudate putamen (CP), the NAc core, and the NAc shell (Figure 5 *A*)—after exposure to varying doses of BRL 5237, a synthetic KOR agonist that mimics the action of endogenous DYN. Because an important role of the DYN/KOR system is to decrease the terminal release of DA (Heijna et al., 1992), it was hypothesized that exposure to BRL 5237 would result in reduced DA release across all animals and all brain regions. We further hypothesized that KOR-rich regions within the striatum would require a smaller concentration of KOR agonist to cause the same relative reduction in DA transmission as regions with less KOR density.

Method

Adult male sexually naïve prairie voles, bred at the University of Michigan, were housed in a 14:10 LD cycle with food and water available *ad libitum*. Subjects were weaned 21 days after birth and housed in same-sex sibling pairs until they were tested as adults around 90 days of age. All experimental procedures were approved by UCUCA at the University of Michigan.

KOR Receptor Autoradiography

At 90 days of age, sexually naïve male voles were sacrificed via rapid decapitation. Brains were quickly removed, frozen on dry ice, and stored at -80°C. Brains were then sectioned on a cryostat at 15 μm in four serial sections (i.e., 60 μm

intervals) and placed back in the -80°C freezer until all samples were ready to be processed. On the day of processing, slides were washed twice in room temperature 50 mM Tris-HCL (pH 7.4) for ten minutes. Samples were then incubated with a KOR ligand (U69,593; cat# NET 952; lot #3615650; PerkinElmer) for two hours. The incubation period was followed by a series of washes that are listed as follows: ice-cold Tris-buffer (2 x 5 minutes), chilled Tris-buffer while stirring (2 x 10 minutes), dip in ice-cold distilled water (3x), and then dried under a cool stream of air. Non-specific binding was determined by incubating a subset of slides with 1 μM nor-BNI for KORs. Kodak BioMax MS Film was then laid on the slides and exposed for six months. Film images were captured using a Scan Maker 1000XL Microtek scanner.

The density of KOR binding was examined in five regions of the striatum (dorsolateral CP, ventrolateral CP, NAc core, dorsomedial NAc shell, and ventral NAc shell) using NIH image v1.42. Results were then analyzed by SPSS v20.0, statistical software designed by IBM, and a Post Hoc Tukey test determined significant differences ($p < .05$) in receptor binding densities.

Electrode Fabrication and Calibration

To create a recording electrode, 1.2 mm glass capillary tubes were filled with a single carbon fiber strand and subsequently placed in a Narashige (Model# PE-22) heated-coil vertical puller to create a seal between the glass and carbon fiber. Next, the carbon fiber was cut under a microscope at a length of 140 ±10 μm beyond the seal. Finally, the electrode was filled with an ionic KCl solution and a silver wire was inserted into the open end of the electrode extending to the bottom, near the seal. The prepared electrode was then placed in a calibration flow cell apparatus, where a 3 μM solution of

DA was applied in flowing calibration aCSF consisting of 126 mM NaCl, 2.5 mM KCl, 1.2 mM NaH_2PO_4, 2.4 mM $CaCl_2$, 1.2 $MgCl_2$, and 25 mM $NaHCO_3$ in deionized H_2O (pH 7.4). Pre-calibration was completed by averaging three readings and taking the resulting current readout (nA) and dividing it by three to quantify the change in current in nAs that corresponded with a 1 μM concentration of DA using FSCV.

FSCV of Coronal Brain Slices.

Following rapid, live decapitation, brains were quickly extracted and immediately submerged in cold, pre-oxygenated high sucrose artificial cerebrospinal fluid (aCSF) consisting of 180 mM sucrose, 30 mM NaCl, 4.5 mM KCl, 1mM $MgCl_2$, 26 mM $NaHCO_3$, 1.2 NaH_2PO_4, and 10 mM D-Glucose in deionized H_2O (pH 7.4). The brain was mounted and sectioned into 400-μm thick coronal slices with a vibratome (Leica VT1200S). Slices containing all three striatal regions (Figure 4 *A*, *dashed red line*)—NAc core, NAc shell, and caudate putamen—at +2.4, +1.60, and +1.20 bregma were then transferred to room temperature aCSF buffer solution consisting of 176.13 mM ascorbate, 180.16 mM glucose, 84.01 mM sodium bicarbonate, 58.44 mM NaCl, 156 mM NaH_2PO_4, 74.56 mM KCl, 147.01 mM $CaCl_2$, and 203.30 mM $MgCl_2$ in deionized H_2O (pH 7.4). After the brain slices were incubated for one hour in an oxygenated holding chamber, one slice was moved to the testing apparatus.

After placing a coronal brain slice in the testing apparatus with a flowing aCSF buffer running at 1 mL/min, a two-pronged, bipolar stimulating electrode and the pre-calibrated recording electrode were lowered onto the brain slice targeting the region of choice (Figure 4 *B*) using an upright microscope for visualization. Using Tarheel CV (University of North Carolina, Chapel Hill) software written in LABVIEW (National

Instruments, Austin, TX), a single reading involved the recording electrode sweeping a triangular ramp from -0.4V to +1.2 V and back, cyclically, at 10Hz for 15 seconds. During this recording, at 5 seconds, the bipolar electrode stimulated the slice, inducing DA release. The characteristic oxidation current, seen at +0.6V during the upward ramp, and reduction current, at -0.2V during the downward ramp, of DA were identified using a background-subtracted cyclic voltammogram (Figure 4 *C, inset*). Throughout testing, slice stimulations occurred at regular five-minute intervals and readings were only recorded for experimental purposes once DA release was consistently stable. After data collection had concluded, the recording electrode was again calibrated in the flow cell apparatus as described above.

KOR Agonist Dose Response

After stabilization, a baseline reading of electrically induced DA release was measured for 30 minutes in flowing aCSF buffer (1mL/min) using FSCV. Then, gradually increasing doses (0.001, 0.01, 0.03, 0.1, 0.3, 1, 3, 10, 20, 30 μM) of KOR agonist BRL 5237 were added to the flowing buffer solution every 30 minutes, again stimulating and recording every 5 minutes. This allowed us to determine the concentration required, per specific recording location within a region, for a 50% reduction in DA transmission (i.e., IC50).

Results were input into the statistical analysis software GraphPad Prism v4.0. Data was averaged within and across animals and normalized to generate KOR agonist dose response curves using non-linear regression with the bottom set equal to 0 to find the average IC50 for a given region and sagittal slice. Because many regions had low

sample sizes, statistics were not run to determine if significant differences were present for IC50s.

Results

KOR Receptor Autoradiography

Receptor autoradiography was used to characterize the distribution of KORs throughout the striatum of male prairie voles. For each of the three striatal regions of interest—the CP, the NAc core, and the NAc shell—KOR distribution was assessed at three different rostro-caudal coordinates relative to bregma: +2.15, +1.60, and +1.20 bregma. This allowed for comparisons within regions of a coronal slice as well as between coronal slices, revealing trends on a, rostral/caudal axis.

In the CP, KOR binding revealed a distinctly higher density of KORs in the lateral regions compared to the medial regions (Figure 1 *A*). So we decided to focus our analysis on the lateral CP, parsing it further into dorsolateral and ventrolateral sub-regions (Figure 1 *B, E, H*). Statistical analysis of KOR density in these regions showed no significant differences between sub-regions within a given coronal slice (Figure 1 *C, F, I*) nor did significant differences in density arise in the same sub-region between the three different coronal slices (Figure 1 *J, K*).

However, KOR autoradiography in the NAc core showed a strong decrease in KOR density moving caudally (Figure 2). Visually, a decreasing trend of KOR density can be spotted in the radiography images of NAc core KOR binding (Figure 2 *A, C, E*). Most notably, the caudal most slice, +1.20 bregma (Figure 2 *E*), has a marked lightness of KOR binding in the core region, whereas the more rostral slices do not. Statistical analysis confirmed this decreasing rostro-caudal gradient in the core (Figure 2 *G*)

showing a significant difference between coronal slices at +2.15 bregma and +1.20 bregma ($p = .001$).

Finally, the NAc shell was separated into dorsomedial and ventral sub-regions since it appeared visually to have two separate KOR density trends. No significant differences were found between sub-regions of a given coronal slice (Figure 3 *C, F, I*), but each sub-region itself showed a clear reduction in KOR density when moving caudally through the striatum (Figure 3 *J, K*); specifically, significant differences were found between the +2.15 and +1.20 bregma coronal slices ($p = .003$, *dorsomedial shell*; $p = .01$, *ventral shell*).

Putting these results together then, it appears that the CP shows increasing KOR binding density when moving medially to laterally within a coronal slice, but shows no trends on the rostro-caudal gradient. On the other hand, both regions of the ventral NAc, the shell and core, show no significant within-slice trends, but both show a KOR density decrease when moving caudally through the striatum.

FSCV KOR Agonist Dose Responses

General trends in DA release in the striatum have been found using FSCV, showing a greater concentration of DA transmission in the CP as compared to the NAc (Trout & Kruk, 1992). Consistent with these findings, we show that DA release decreases when moving from the CP to the NAc core, and on to the NAc shell (Figure 5). Moreover, our identification of DA as the released neurotransmitter (Figure 4 *C, inset*) is consistent with results seen for *in vivo* FSCV DA studies (Robinson et al., 2003). Armed with the KOR receptor autoradiography data, we moved on to quantifying the effects of KOR activation on DA release using FSCV (Figure 4). Broadly speaking, our results

align with the biological distribution of KOR receptors found in our receptor autoradiography—that is to say that in regions that appeared KOR-rich, less KOR agonist was needed to affect a 50% reduction in DA release.

Specifically, in the lateral CP, no consistent trend was found either between sub-regions or between coronal slices (Figure 6). Neither selectivity on the rosto-caudal gradient nor sub-regional localization within a slice affected KOR's effect on DA transmission. Considering IC50 discrepancies were highest in recordings that were very close in proximity on the same coronal slice (Figure 6 *C*, *E*), natural variation in the vole population would be the most parsimonious explanation for such results. The relative similarity of IC50 concentrations between coronal slices aligns nicely with the autoradiography data KOR density data, which showed no significant rostro-caudal differences.

Aligning with autoradiography results, the FSCV findings within the NAc core showed a strong trend of increasing dosage required for an IC50 when moving caudally (Figure 7 *B, D, F; IC50s in red*). Where KOR density seemed to be the lightest (Figure 2 *E*), the highest concentration of KOR agonist was needed to cause a 50% reduction in DA transmission (Figure 7 *F; IC50 in red*). While the sample size is too small to provide statistical comparisons between coronal slices, it appears that the ideal slice for examining the KOR/DA interaction in the core is the rostral most, +2.15 bregma. Future studies will increase the number of recordings and will determine if the trends described here stand the test of time.

In the NAc shell, the receptor autoradiography showed a decreasing rostro-caudal density trend. However, FSCV KOR dose response data, however, did not follow this

clear trend (Figure 8). While the caudal most slice showed a high concentration of KOR agonist required for an IC50 (Figure 8 *E, F*), the +1.60 bregma, middle slice (Figure 8 *C, D*), and not the most rostral slice (Figure 8 *A,* B) as would have been expected by KOR autoradiography, appeared to be the sweet spot of KOR inhibitory activity. As with data from the core, more experimentation is needed before confidently determining the relationship between KOR binding and DA transmission.

In summary, the lateral CP, showed no trends within slices, nor were any significant differences found on the rosto-caudal axis. The NAc core showed a marked decrease in core density moving caudally, so the ideal slice, requiring the least concentration of KOR agonist, was the rostral most at +2.15 bregma. Surprisingly, in the shell, an FSCV sweet spot was found at +1.60 bregma on the rostro-caudal gradient in the ventral shell sub-region.

Discussion

Previous and ongoing work in our laboratory has demonstrated that aversive motivation, mediated by interactions between KOR and DA systems, is very important for the regulation of social attachments. Here, determined to better understand the interactions between these systems, novel investigations into the anatomical topography and corresponding neurochemical interaction were conducted in multiple compartments of the striatum of sexually naïve voles. By integrating both receptor autoradiography and FSCV, we were able to locate the specific striatal sub-regions where the modulation of DA transmission by the DYN/KOR system appears to be the strongest. These results were highly congruent with trends we saw in our KOR autoradiography data. As hypothesized, our FSCV data showed that KOR activation resulted in decreased

dopaminergic output and this inhibition showed greatest enhancement within regions of high KOR density. Briefly, our data suggests that the rostral most regions of the striatum (~+2.15 bregma) and, even more specifically, the ventral striatum (i.e. containing the NAc and not the CP) appears to be where KORs have the most robust modulation of DA transmission.

Interestingly, KOR distribution between other rodent species shows variance in the striatum. Rats, rabbits and guinea pigs, all show varying degrees of overall KOR striatal expression (Robson et al., 1985). Humans show relative consistency across the striatum, with marked heterogeneity in the caudate (Quirion et al, 1987), which is a strikingly similar finding to the lack of significant variation we discovered in the vole CP. Still, no studies to date have directly compared KOR distribution between voles and humans or animals of other species.

Future studies will first need to replicate the present findings so that we may gain confidence in the robustness of our data. Once certain about the KOR/DA interaction in the specific sub-regions of the vole striatum, behavioral studies will need to be conducted to determine if this location is important for interactions between these two systems with respect to regulation of social attachment behaviors, including the formation and maintenance of monogamous pair bonds.

Specifically, we can examine whether and how the biochemistry of the KOR/DA interaction differs between pair bonded and sexually naïve voles. We know that both D_1-like receptor activation and KOR receptor activation play integral roles in the selective aggression shown by pair bonded subjects (Aragona et al., 2006). Because low-affinity D_1-like receptors require higher concentrations of DA to become activated (Richfield et

al., 1989), pair bonded voles may show enhanced DA transmission. Activation of D_1-like receptors ultimately leads to KOR activation via enhanced DYN activity (Gerfen et al., 1991). Theoretically then, in a resident-intruder paradigm, a pair bonded vole may see a greater surge in DA when happening upon an unfamiliar vole initially motivating it to pay more attention to this novel stimuli; then, after the downstream effects of D_1 receptor activation kick in, enhanced KOR activation could lead to aggressive rejection. Additionally, like D_1 receptor density, KOR topography could be altered after formation of a pair bond; yet another piece of the puzzle requiring investigation. Because the modulatory effect of the κ-opioid system on DA transmission plays such a critical role in pair bonding, slice FSCV comparing differences between pair bonded and sexually naïve voles is a valuable tool for accessing the neurochemistry of this behavior.

Furthermore, it is quite possible that neuroanatomical restructuring of KOR or DYN expression may occur in chronically stressed or drug addicted subjects, as has been seen in humans (Hurd & Herkenham, 1993; Frankel et al., 2008; Wee & Koob, 2010). Perhaps, like its protective effects on drug addiction in voles (Ito et al., 2004; Liu et al., 2011), formation of social attachment can be shown to buffer the effects of aversion-induced stress on dopaminergic activity through a KOR mediated pathway. Our current study lays the necessary groundwork for evaluating all of these suggested future experiments.

Also, another, significantly more time consuming, study could build on our results by leveraging bi-lateral symmetry in the brain to find the exact KOR density at the site of recording. By punching out a small section of tissue in the opposite hemisphere in the same region and coronal slice as the FSCV reading, methods such as RT-PCR can

quantify the amount of KOR mRNA (Peng et al., 2012) at a site analogous to the FSCV recording. With this data, we could control perfectly for individual variation and get a sense of how activity varies between sexually naïve and pair bonded voles. So, DA transmission results could be standardized across all animals.

In neuroscience, our scientific endeavors aim to shed light on the mysteries of the human condition. We hope that by using appropriately analogous animal subjects and experimental manipulations that we can learn something about ourselves. The present study opens a scientific door; it allows us to further examine the neurochemistry of aversive and stressful states and future studies will be able to evaluate how the influence of a stable social bond affects it. It takes little imaginative flexibility to find anecdotal evidence for the importance of social bonds in our daily lives. As such, this line of research is a beacon of potential for discovering and perhaps one day clinically utilizing the underlying mechanisms that shape our behavior.

References

Aragona, B.J., Liu, Y., Yu, Y.J., Curtis, J.T., Detwiler, J.M., Insel, T.R., & Wang, Z. (2006). Nucleus accumbens dopamine differentially mediates the formation and maintenance of monogamous pair bonds. *Nature Neuroscience*, *9*(1), 133-139.

Aragona, B.J., & Wang, Z. (2009). Dopamine regulation of social choice in a monogamous rodent species. *Frontiers in Behavioral Neuroscience*, *3*(15), 1-11.

Atzil, S., Hendler, T., & Feldman, R. (2011). Specifying the neurobiological basis of human attachment: Brain, hormones, and behavior in synchronous and intrusive mothers. *Neuropsychopharmacology*, *36*(13), 2603-15.

Becker, J.B., Rudick, C.N., & Jenkins, W.J. (2001). The role of dopamine in the nucleus accumbens and striatum during sexual behavior in the female rat. *The Journal of Neuroscience*, *21*(9), 3236-41.

Berridge, K.C., & Robinson, T.E. (1998). What is the role of dopamine in reward: Hedonic impact, reward learning, or incentive salience? *Brain Research*, *28*(3), 309-69.

Carter, C.S., & Getz, L.L. (1993). Monogamy and the prairie vole. *Scientific American*, *268(6)*, 100-106.

Chavkin, C., James, I.F., & Goldstein, A. (1982). Dynorphin is a specific endogenous ligand of the kappa opioid receptor. *Science*, *215*, 413-15.

Chefer, V.I., Czyzyk, T., Bolan, E.A., Moron, J., Pintar, J.E., & Shippenberg, T.S. (2005). Endogenous kappa-opioid receptor systems regulate mesoaccumbal dopamine dynamics and vulnerability to cocaine. *The Journal of Neuroscience*, *25*(20), 5029-37.

Dewsbury, D.A. (1987). The comparative psychology of monogamy. *Nebraska Symposium on Motivation*. *35,* 1-50.

Frankel, P.S., Alburges, M.E., Bush, L., Hanson, G.R., & Kish, S.J. (2008). Striatal and ventral pallidum dynorphin concentrations are markedly increased in human chronic cocaine users. *Neuropharmacology*, *55*(1), 41-6.

Gavish, L., Carter, C.S., & Getz, L.L. (1983). Male-female interactions in priairie voles. *Animimal Behavior*, *31*, 511-17.

Gerfen, C.R., McGinty, J.F., & Young, W.S. (1991). Dopamine differentially regulates dynorphin, substance P, and enkephalin expression in striatal neurons: in situ hybridization histochemical analysis. *The Journal of Neuroscience*, *11*, 1016-31.

Heijna, M.H., Bakker, J.M., Hogenboom, F., Mulder, A.H., & Schoffelmeer, A.N. (1992). Opioid receptors and inhibition of dopamine-sensitive adenylate cyclase in slices of rat brain regions receiving a dense dopaminergic input. *European Journal of Pharmacology*, *229*(2-3), 197-202.

Hurd, Y.L., & Herkenham, M. (1993). Molecular alterations in the neostriatum of human cocaine addicts. *Synapse, 13*, 357–69

Insel, T.R., & Hulihan, T.J. (1995). A gender-specific mechanism for pair bonding: oxytocin and partner preference formation in monogamous voles. *Behavioral Neuroscience*, *109*(4), 782-89.

Insel, T.R., Preston, S., & Winslow, J.T. (1995). Mating in the monogamous male: Behavioral consequences. *Physiology & Behavior*, *57*(4), 615-27.

Ito, R., Robbins, T.W., & Everitt, B.J. (2004). Differential control over cocaine-seeking behavior by nucleus accumbens core and shell. *Nature Neuroscience*, *7*, 389-97.

Kelley, A.E., & Berridge, K.C. (2002). The neuroscience of natural rewards: relevance to addictive drugs. *The Journal of Neuroscience*, *22*(9), 3306-11.

Kleiman, D. (1977). Monogamy in mammals. *Quarterly Reviews of Biology*, *52*, 39-69.

Knoll, A.T., & Carlezon, W.A. (2010). Dynorphin, stress, and depression. *Brain Research*, *1314*, 56-73.

Land, B.B., Bruchas, M.R., Lemos, J.C., Xu, M., Melief, E.J., & Chavkin, C. (2008). The dysphoric component of stress is encoded by activation of the dynorphin kappa-opioid system. *The Journal of Neuroscience*, *28*, 407-14.

Liu, Y., Young, K.A., Curtis, J.T., Aragona, B.J., & Wang, Z. (2011). Social bonding decreases the rewarding properties of amphetamine through a dopamine D1 receptor-mediated mechanism. *The Journal of Neuroscience*, *31*(22), 7960-66.

Mansour, A., Khachaturian, H., Lewis, M.E., Akil, H., & Watson, S.J. (1987). Autoradiographic differentiation of mu, delta, and kappa opioid receptors in the rat forebrain and midbrain. *The Journal of Neuroscience*, *7*, 2445-64.

Mansour, A., Khachaturian, H., Lewis, M.E., Akil, H., & Watson, S.J. (1988). Anatomy of CNS opioid receptors. *Trends in Neurosciences*, *11*, 308-14.

McLaughlin, J.P. Marton-Popovici, M., & Chavkin, C. (2003). K-Opioid receptor antagonism and prodynorphin gene distribution block stress-induced behavioral responses. *The Journal of Neuroscience*, *23*(14), 5674-83.

Nestler, E.J., & Carlezon, W.A. (2006). The mesolimbic dopamine reward circuit in depression. *Society of Biological Psychiatry*, *59*, 1151-59.

Peng, J., Sarkar, S., & Chang, S. L. (2012). Opioid receptor expression in human brain and peripheral tissues using absolute quantitative real-time RT-PCR. *Drug and alcohol dependence*, 1-6.

Quirion, R., Pilapil, C., & Magnan, J. (1987). Localization of kappa opioid receptor binding sites in human forebrain using [3H]U69,593: Comparison with [3H]bremazocine. *Cellular and Molecular Neurobiology, 7*, 303-07.

Ravitz, P., Maunder, R., Hunter, J., Sthankiya, B., & Lancee, W. (2010). Adult attachment measures: a 25-year review. *Journal of Psychosomatic Research*, *69*(4), 419-32.

Richfield, E.K., Penney, J.B., & Young, A.B. (1989). Anatomical and affinity state comparisons between dopamine D1 and D2 receptors in the rat central nervous system. *Neuroscience*, *30*, 767–77.

Robinson, D.L., Venton, B.J., Heien, M.L., & Wightman, R.M. (2003). Detecting subsecond dopamine release with fast-scan cyclic voltammetry in vivo. *Clinical Chemistry*, *49*(10), 1763-73.

Robson, L.E., Gillan, M.G., & Kosterlitz, H.W. (1985). Species differences in the concentrations and distributions of opioid binding sites. *European Journal of Pharmacology, 112*, 65-71.

Steiner, H., & Gerfen, C.R. (1995). Dynorphin opioid inhibition of cocaine-induced, D1 dopamine receptor-mediated immediate-early gene expression in the striatum. *The Journal of Comparative Neurology*, *353*, 200-212.

Trout, S.J., & Kruk, Z.L. (1992). Differences in evoked dopamine efflux in rat caudate putamen, nucleus accumbens and tuberculum olfactorium in the absence of

uptake inhibition: Influence of autoreceptors. *British Journal of Pharmacology*, *106*(2), 452-58.

Wang, Y.J., Rasakham, K., Huang, P., Chudnovskaya, D., Cowan, A., & Liu-Chen, L.Y. (2011). Sex difference in kappa-opioid receptor (KOPR)-mediated behaviors, brain region KOPR level and KOPR-mediated guanosine 5'-O-(3-[35S]thiotriphosphate) binding in the guinea pig. *The Journal of Pharmacology and Experimental Therepeutics*, *339*, 438-5.

Wee, S., & Koob, G. F. (2010). The role of the dynorphin-kappa opioid system in the reinforcing effects of drugs of abuse. *Psychopharmacology*, *210*(2), 121-35.

Williams, J.R., Catania, K.C., & Carter, C.S. (1992). Development of partner preferences in female prairie voles (Microtus ochrogaster): The role of social and sexual experience. *Hormones and behavior*, *26*(3), 339-49.

Winslow, J.T., Hastings, N., Carter, C.S., Harbaugh, C.R., & Insel, T.R. (1993). A role for central vasopressin in pair bonding in monogamous prairie voles. *Nature*, *365*, 545-48.

Author Note

Zubin Sedghi, Department of Neuroscience, The University of Michigan

First, I would like to thank my mentor Dr. Brandon Aragona, who provided the insight, advice, and encouragement necessary to complete this study. His passion is apparent, among other things, in his meticulous and thoughtful pursuit of scientific investigation. I owe to him this invaluable experience in research. Thank you.

In an infinitesimally close second comes Shanna Harkey (Resendez) without whom my work would also not be possible. She played an integral role every step of the way, including much needed support and guidance in the trenches of voltammetry. I can't say or do enough to thank her and I am excited for her exceedingly bright future as a primary investigator of her own lab (with a retractable roof)!

Also, thanks go to Caitlin Vander Weele for her advice and help with the thesis-writing process and for constantly answering the question: "Where is the (fill in any/all lab equipment here)?" Her patience and guidance are both appreciated.

I would be remiss not to thank my all of my fellow undergraduate lab mates, particularly Curtis Austin and Gwen Gormley. Thank you so much for all of your help.

Finally, special thanks go to my parents, brother and girlfriend who not only provided moral support, but also allowed me to frequently recede into my research-related hermit cave!

(Honorable Mentions: Ronald and Tina)

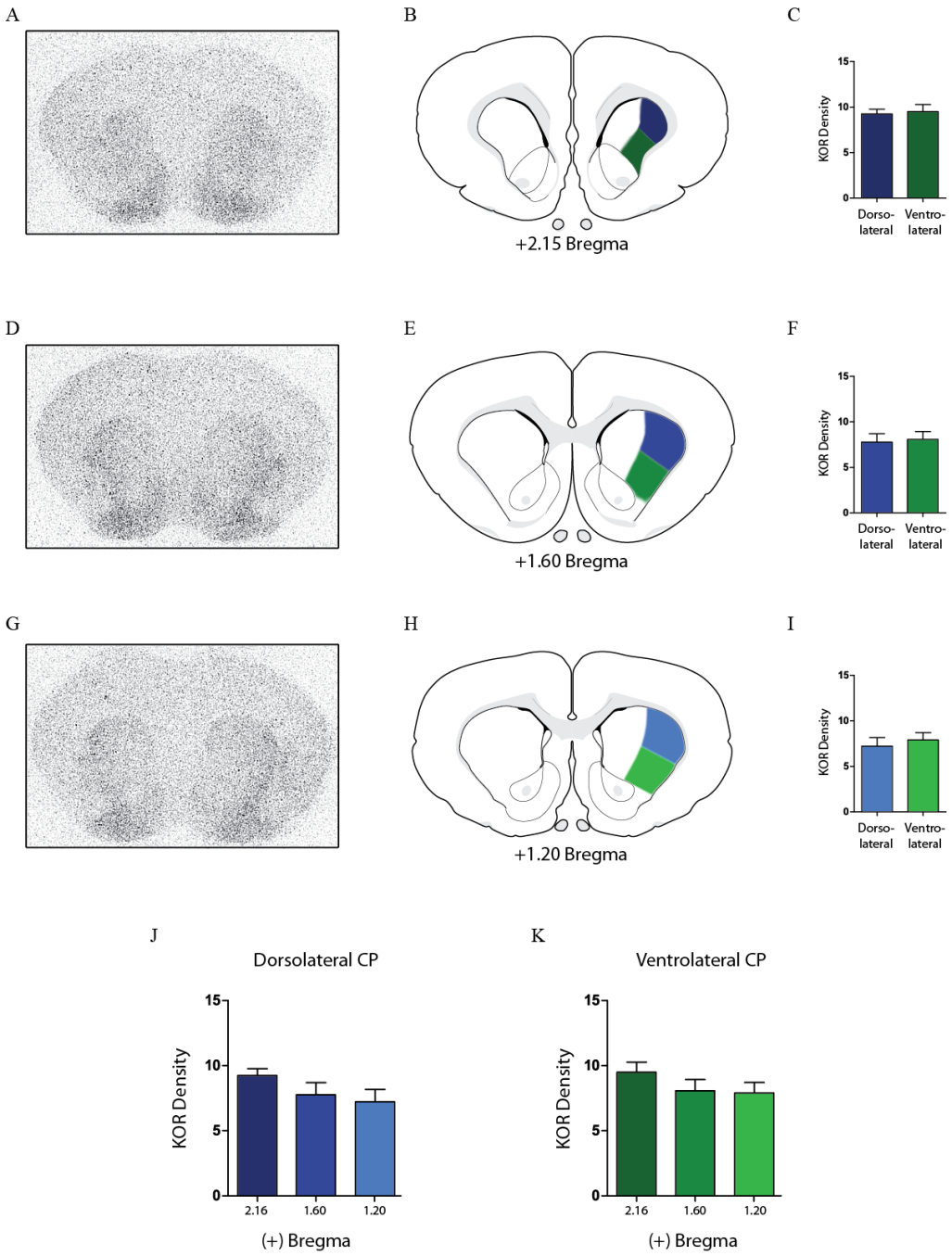

Figure 1. KOR Receptor Autoradiography in the CP. **A., D., G.** KOR receptor autoradiography for coronal slices at +2.15, +1.60, and +1.20 bregma respectively. **B., E., H.** Illustrated schematics of high-density sub-regions within the CP. Dorsolateral CP (blue) and ventrolateral CP (green) represent the areas that were analyzed for KOR density. **C., F., I.** Graphs comparing KOR density between sub-regions within a given coronal slice. No significant differences were found. **J.** Dorsolateral and **K.** ventrolateral KOR densities compared between coronal slices, which become progressively caudal from left to right. No significant differences were found.

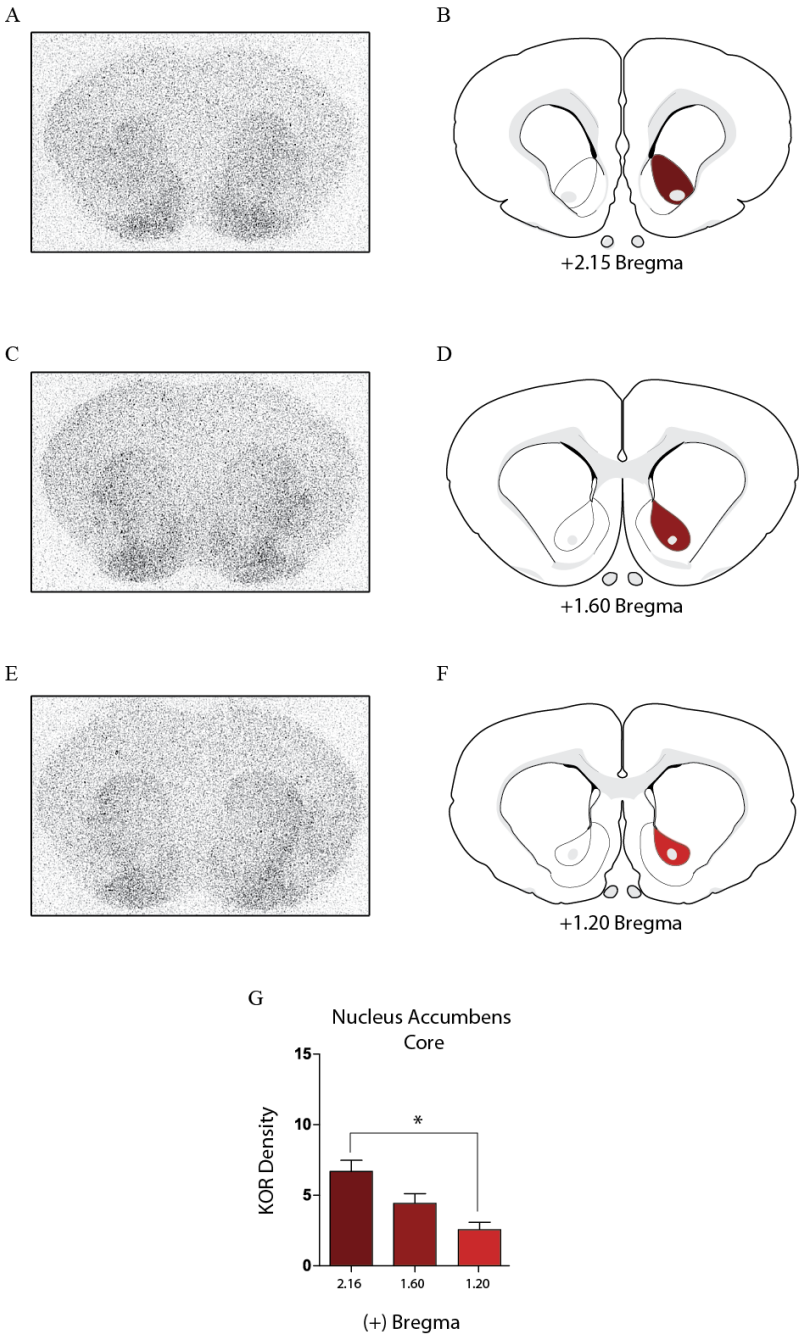

Figure 2. KOR Receptor Autoradiography in the NAc Core. **A., C., E.** Visualized KOR receptor autoradiography for coronal slices at +2.15, +1.60, and +1.20 bregma respectively. The caudal most slice (**E.**) shows a noticeable decrease in KOR density in the NAc core. **B., E., F.** Illustrated schematics of the NAc core in each coronal slice (red). **G.** Quantification of KOR densities in the NAc core. Coronal slices, from which KOR density was analyzed, become progressively more caudal moving left to right. The core at +1.20 bregma had significantly fewer KOR receptors than the core at +2.15 bregma (p = .001) showing a rostral to caudal decrease in KOR density.

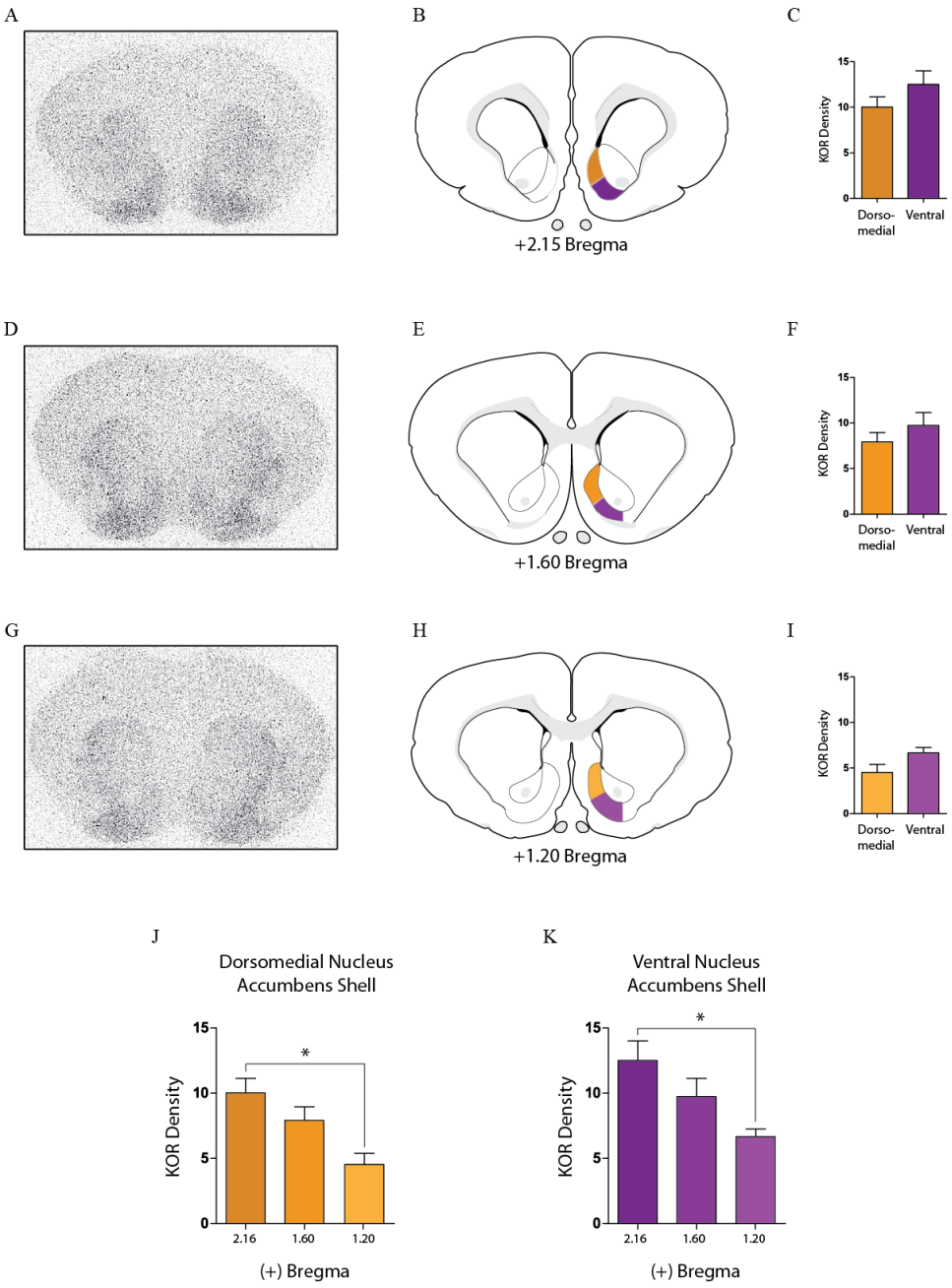

Figure 3. KOR Receptor Autoradiography in the NAc Shell. **A., D., G.** KOR receptor autoradiography for coronal slices at +2.15, +1.60, and +1.20 bregma respectively. **B., E., H.** Illustrated schematics of sub-regions within the shell. Dorsomedial (yellow) and ventral (purple) shell represent the areas analyzed for KOR density. **C., F., I.** Density comparisons between sub-regions within a given coronal slice. No significant differences were found. **J.** Dorsomedial and **K.** ventral shell KOR densities compared between sagittal slices. A significant difference appears for each sub-regions between +2.15 and +1.20 bregma (*dorsomedial shell, p* = .003; *ventral shell, p* = .01), suggesting a rostro-caudal decrease in KOR density for the NAc shell.

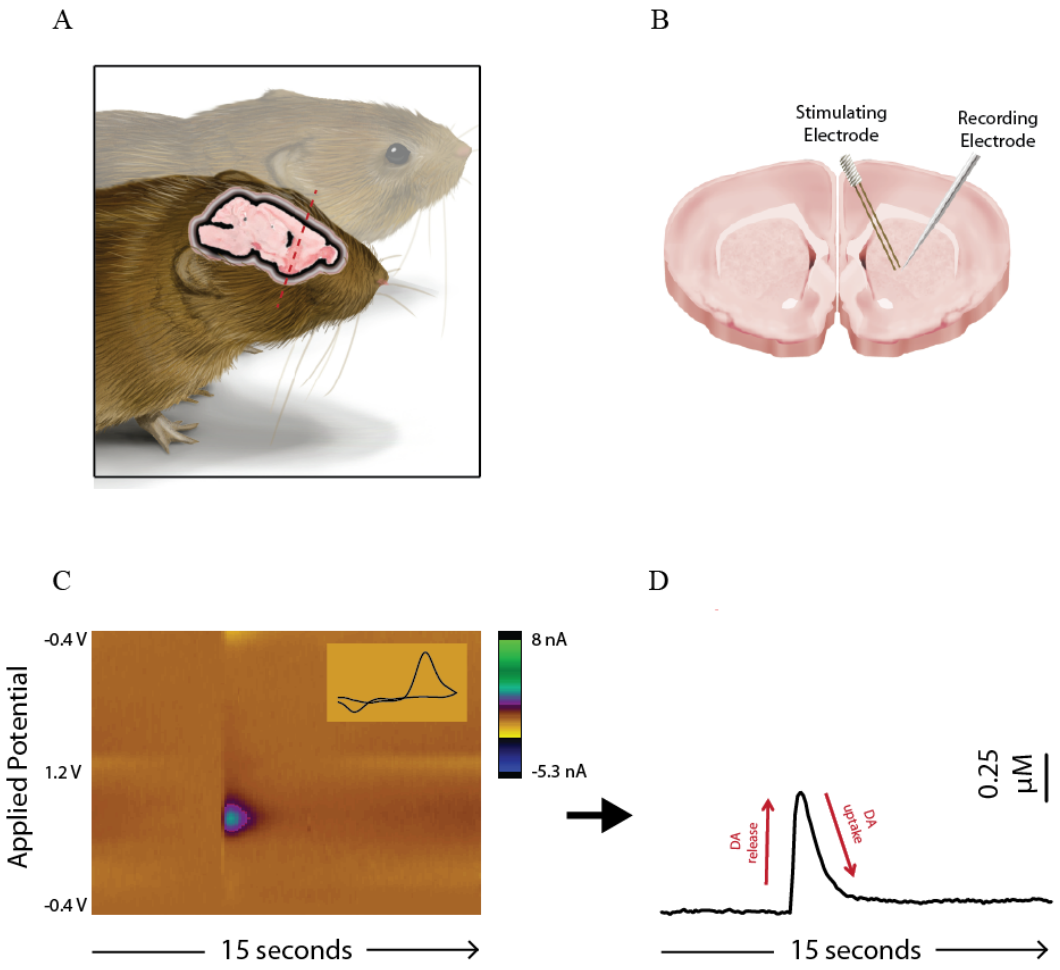

Figure 4. FSCV Basics. **A.** Sagittal brain slice depicted in its approximate location in the prairie vole head. The red dotted line indicates the prime location for finding all three striatal regions, corresponding to the depth from which coronal slices were used for testing. **B.** Coronal brain slice, 400 µM thick, showing a two-pronged, stimulating electrode and a recording electrode lowered for experimentation. **C.** Color plot showing the current for all 15 seconds of a measurement. At 5 seconds the stimulating electrode activates, causing a release of DA, which is detected by the recording electrode. The inset shows the characteristic cyclic voltammogram for DA with its oxidation peak on the right and the reduction dip on the left. **D.** A view of the concentration of DA that is released by a single stimulation of the slice.

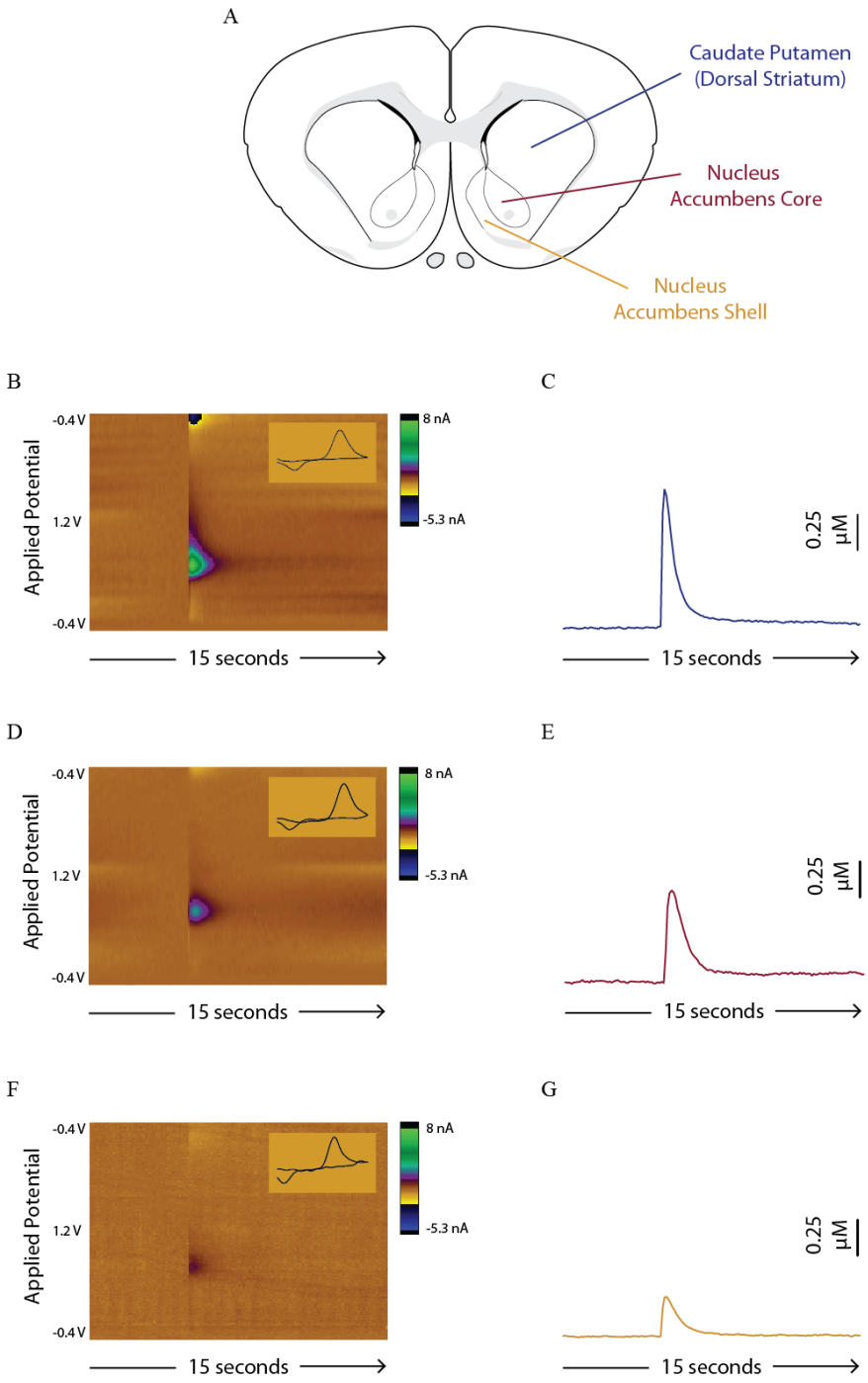

Figure 5. Comparison of FSCV DA release in three striatal regions. **A.** A coronal brain slice illustration indicates the anatomical locations of the CP, the NAc core, and the NAc shell. **B., D., F.** Color plots of a single stimulation and recording of DA release in the CP, NAc core, and NAc shell respectively. **C., E., G.** Graphs showing the concentration of dopamine released in the CP, NAc core, and NAc shell. Notice a decrease in DA release from the CP to the NAc core and again from the NAc core to the NAc shell.

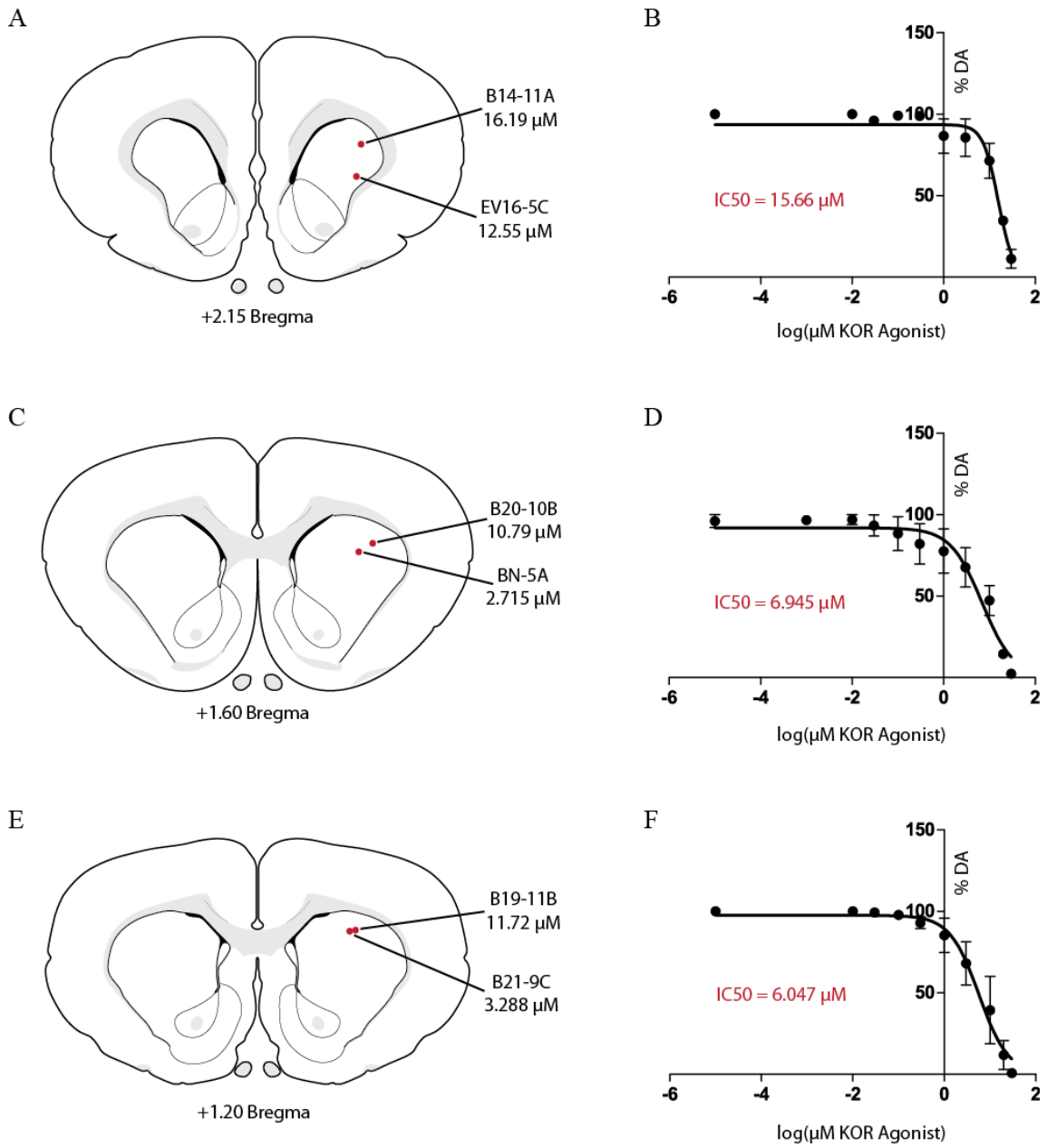

Figure 6. FSCV KOR Agonist Dose Responses in the CP. **A., C., E.** 3 different coronal slices, moving caudally in the brain from slice (**A.**) to slice (**E.**). Red dots connote the location of each recording electrode, and beside each is the assigned name of the subject with the IC50 concentration of KOR agonist required to see a 50% reduction in DA transmission. **B., D., F.** Normalized dose response curves generated from all animals on a respective coronal slice. In red, the combined IC50 is given for each coronal depth. No trend can be found on the rostral to caudal gradient, consistent with KOR receptor autoradiography findings.

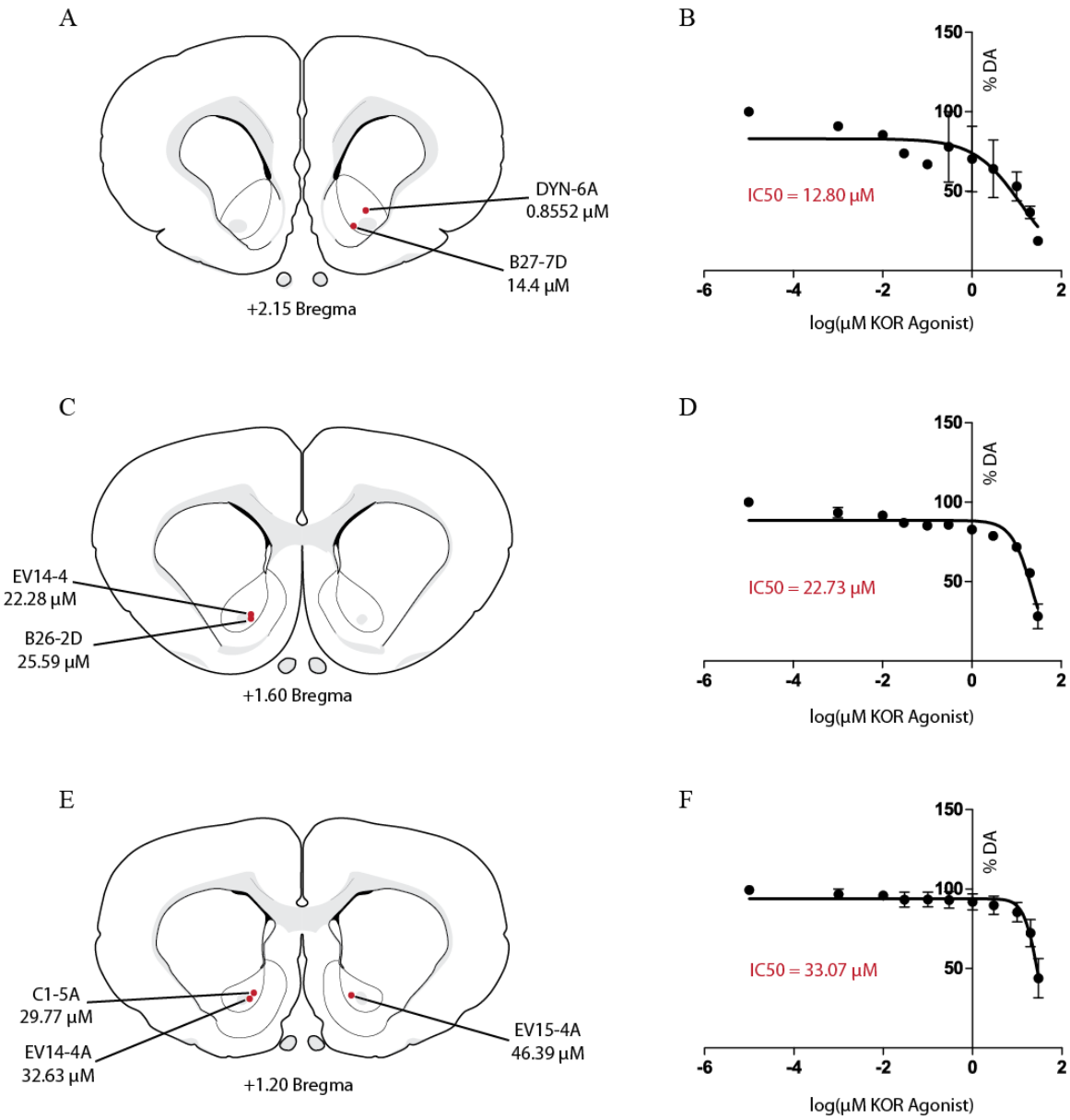

Figure 7. FSCV KOR Agonist Dose Responses in the NAc Core. **A., C., E.** 3 different coronal slices, moving caudally in the brain from slice (**A.**) to slice (**E.**). Red dots connote the location of each recording electrode, and beside each is the assigned name of the subject with the IC50 concentration of KOR agonist required to see a 50% reduction in DA transmission. **B., D., F.** Normalized dose response curves generated from all animals on a respective coronal slice. In red, the combined IC50 is given for each coronal depth. A trend formed on the rostro-caudal gradient requiring more KOR agonist to cause a 50% decrease when moving caudally. The results are consistent with KOR autoradiography in the NAc core, which shows a decrease in KOR receptors moving caudally.

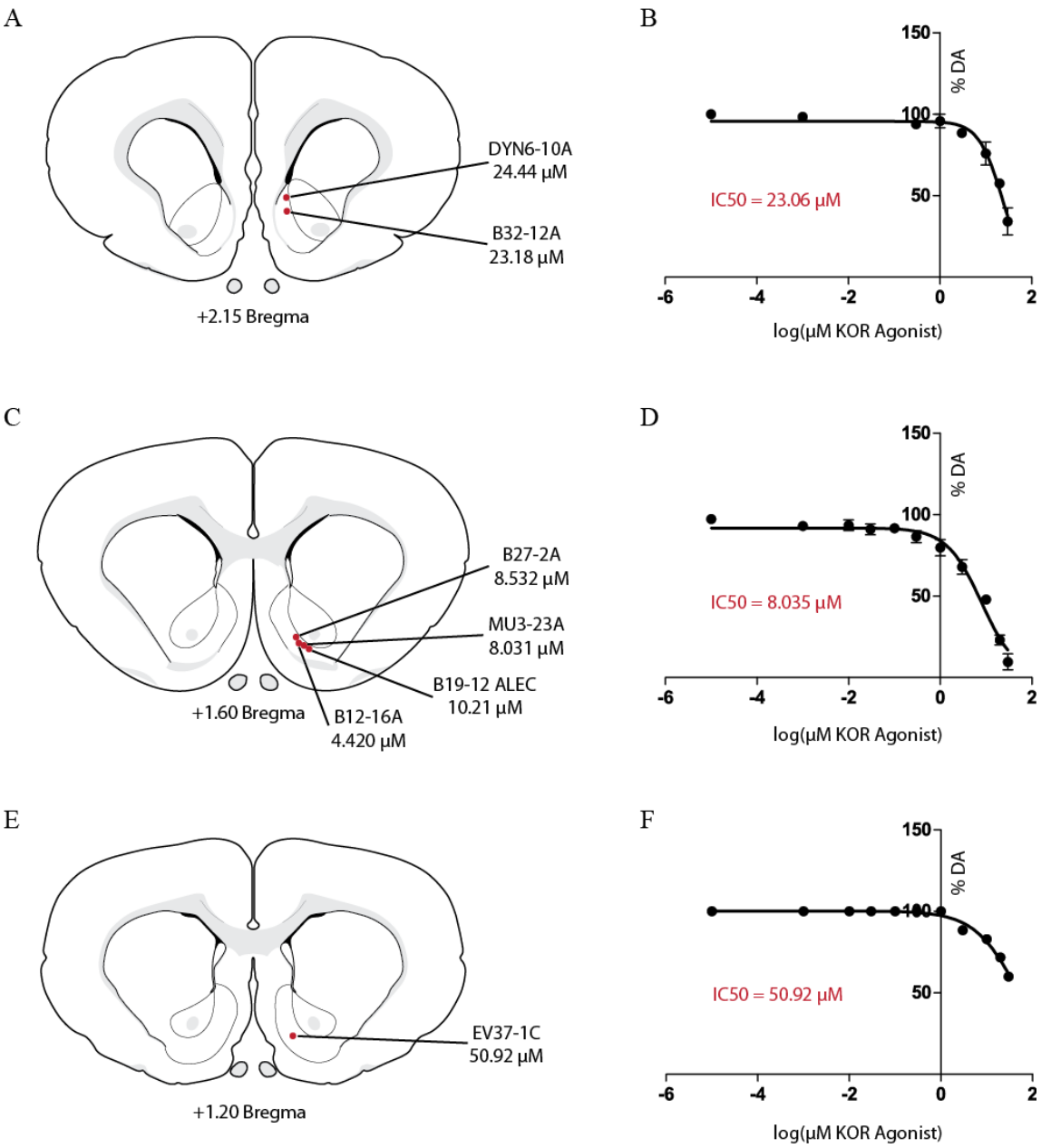

Figure 8. FSCV KOR Agonist Dose Responses in the NAc Shell. **A., C., E.** 3 different coronal slices, moving caudally in the brain from slice (**A.**) to slice (**E.**). Red dots connote the location of each recording electrode, and beside each is the assigned name of the subject with the IC50 concentration of KOR agonist required to see a 50% reduction in DA transmission. **B., D., F.** Normalized dose response curves generated from all animals on a respective coronal slice. In red, the combined IC50 is given for each coronal depth. Preliminary results show peak KOR action, and therefore ideal recording location, in the shell to be in the ventro-lateral sub-region at +1.60 bregma.